Published in final edited form as:
Biomaterials. 2011 November ; 32(31): 7774–7784. doi:10.1016/j.biomaterials.2011.06.075.

Carboxyl-Ebselen-Based Layer-by-Layer Films as Potential Antithrombotic and Antimicrobial Coatings

Wenyi Cai[1], **Jianfeng Wu**[2], **Chuanwu Xi**[2], **Arthur J. Ashe III**[1], and **E. Meyerhoff Mark**[1,*]

[1]Department of Chemistry, The University of Michigan, Ann Arbor, MI, 48109, USA

[2]Department of Environmental Health Sciences, The University of Michigan, Ann Arbor, MI, 48109, USA

Abstract

A carboxyl-ebselen-based layer-by-layer (LbL) film was fabricated by alternatively assembling carboxyl-ebselen immobilized polyethylenimine (e-PEI) and alginate (Alg) onto substrates followed by salt annealing and cross-linking. The annealed films exhibiting significantly improved stability are capable of generating nitric oxide (NO) from endogeneous *S*-nitrosothiols (RSNOs) in the presence of a reducing agent. The NO generation behaviors of different organoselenium species in solution phase are compared and the annealing mechanism to create stable LbL films is studied in details. An LbL film coated polyurethane catheter is capable of generating physiological levels of NO from RSNOs even after blood soaking for 24 h, indicating potential antithrombotic applications of the coating. Further, the LbL film is also demonstrated to be capable of reducing living bacterial surface attachment and killing a broad spectrum of bacteria, likely through generation of superoxide ($O_2^{\bullet -}$) from oxygen. This type of film is expected to have potential application as an antithrombotic and antimicrobial coating for different biomedical device surfaces.

Keywords

Nitric oxide; Superoxide; Thrombosis; Biocompatibility; Antimicrobial

1. Introduction

Thrombus formation and bacterial infection are two common problems that lead to complications of blood-contacting biomedical devices such as catheters, vascular grafts and heart valves [1, 2]. Developing antithrombotic and antimicrobial coatings is of paramount importance to sustain the functionality of such biomedical devices, and thereby reduce the mortality rate and medical costs due to complications.

Incorporating antithrombotic and antimicrobial agents into the surface coating has proven to be an effective strategy to reduce thrombus formation or bacterial infection related complications. For example, heparin-immobilized catheters have been commercialized [1]

Corresponding author: Mark E. Meyerhoff, Department of Chemistry, The University of Michigan, 930 N University, Ann Arbor, MI, 48109, Telephone: +1-734-763-5916, mmeyerho@umich.edu.

and biocidal coatings based on antibiotics and silver species have also been developed [3, 4]. Recently, nitric oxide (NO) has been demonstrated to be a potent anti-platelet and antimicrobial agent that can prevent thrombus formation [5, 6] and reduce bacterial adhesion [6, 7]. Artificial surfaces with equivalent or higher NO fluxes compared to healthy endothelial cells, the most non-thrombogenic surfaces known with NO fluxes of $0.5\sim4\times10^{-10}$ mol cm^{-2} min^{-1}, are expected to have similar antithrombotic properties [8]. Although polymeric coatings based on synthetic NO donors like diazeniumdiolates (NONOates) do exhibit significant anti-thrombotic [5] and antimicrobial properties [9], the toxicity of some diazeniumdiolates and the potential formation of carcinogenic nitrosamines *in-vivo* has thus far greatly limited their clinic applications [10].

S-nitrosothiols (RSNOs), such as *S*-nitrosoglutathione (GSNO) and *S*-nitrosocysteine (CysNO), are a group of endogeneous NO donors that are present in blood. NO can be generated from RSNOs through heat, light or catalyst-initiated decomposition [11]. Recently, RSNO modified xerogel films with low toxicity have shown to exhibit antithrombotic and antimicrobial properties [6]. Despite the reduced toxicity, the limitation of the RSNO-based NO release coatings, however, comes from the limited NO reservoir that could be incorporated into the polymer matrix. With the depletion of NO donors, the NO release decreases over time, resulting in a short life-time for this type of coating. Meanwhile, since most of the RSNO-releasing coatings rely on heat or light-induced RSNO decomposition, the clinic application is limited due to the ineffectiveness of heat-induced RSNO decomposition under physiological conditions and the denied access to light for indwelling biomedical devices. In addition, the instability of RSNOs in the presence of heat, light, pH change and trace metal ions also renders difficulties in the storage of this type of coatings [11].

As an alternative to incorporating NO donors into the polymeric coatings, NO generation materials, a group of catalyst-based coatings, are capable of generating NO when endogenous RSNOs are present as the substrate. It has been shown that glutathione peroxidase (GPx), a selenoenzyme that protects cell from oxidation stress by reducing hydroperoxides using glutathione (GSH), can convert RSNO into NO. Organoselenium species that act as GPx mimics like selenocystamine (SeCA, Fig. 1A) and 3, 3′-dipropionicdiselenide (SeDPA, Fig. 1B), have also exhibited RSNO decomposition activities. In the presence of reducing agents at neutral pH, the diselenides can be converted into selenolates, which are the key intermediates that can reduce RSNOs into NO and thiolates [12]. Interestingly, the reaction of selenolate with oxygen is also known to produce superoxide ($O_2^{\bullet-}$), which is able to inhibit bacterial adhesion to the surface [13]. However, a recent study has shown that the reaction between aliphatic selenolates and oxygen is so fast that a significant amount of superoxide ($O_2^{\bullet-}$) and selenenyl radical (RSe•) are produced, and the accumulation of toxic peroxides and radical species through further reactions leads to the known toxicity of aliphatic selenium species [14]. Aliphatic selenium species are also known to trigger thiol medicated one electron reduction of certain enzymes like cytochrome C, which also contributes to their toxicity [15]. Consequently, the *in-vivo* toxicity of alkyldiselenides greatly limits their potential biomedical applications, and aromatic selenium species, with reduced electron density on the selenium and reduced reactivity, have proven to be less toxic than their aliphatic counterparts. Recently, a series of aromatic selenium species, with good GPx activity and reduced *in-vivo* toxicity, have been developed. For example, the drug ebselen (2-phenyl-1,2-benzisoselenazol-3-(2H)-one, Fig. 1C), is undergoing phase III clinic trial in Japan due to its low toxicity, anti-inflammatory and anti-oxidation properties [15]. The antimicrobial activity of ebselen and its derivatives have also been reported [16–18]. The catalytic activity of these species for RSNO decomposition, however, has not been examined.

Layer-by-Layer (LbL) assembly has become a powerful and versatile technique for surface modification [19]. Based on electrostatic, hydrophobic and a variety of other interactions, this method is applicable for different building blocks and substrates. The self-assembly nature and simplicity in the dip-coating procedures of this method enables the utilization of automatic LbL assembly systems. Considering various materials that can be applied as the substrates, LbL assembly can be a universal and convenient method to apply coatings on biomedical devices. Recently, we reported the use of a LbL film containing aliphatic diselenide species for NO generation [20]. However, the stability of the conventional LbL films is highly related to factors such as pH and ionic strength. The *in-vivo* toxicity also limits the applications of the aliphatic selenium species-based-LbL coatings.

Herein, the NO generation catalytic activity of different organoselenium species for RSNO decomposition is studied and compared. By covalently attaching carboxyl-ebselen (C-ebselen, Fig. 1D) to polyethylenimine (PEI), ebselen-PEI (e-PEI, Fig. 1E), a water-soluble NO generation polymer is obtained. C-ebselen-based LbL films are fabricated by alternatively assembling the resulting e-PEI and sodium alginate (Alg) onto a suitable substrate and further annealed to obtain a more robust and stable film with minimal Se leaching. The annealing mechanism is studied in detail. Finally, the NO generation and antimicrobial properties of the final LbL films are also examined.

2. Materials and Methods

2.1 Materials

SeDPA were synthesized using reported method [12]. Ebselen, 1-(3-dimethylaminopropyl)-3-ethylcarbodiimide (EDC), N-hydroxysuccinimide (NHS), 2-(N-morpholino)ethanesulfonic acid (MES), rhodamine B (RB), fluorescein-5-thiosemicarbazide (FTSC), redistilled nitric acid (≥99.999% trace metals basis), polyethyleneimine (PEI, Mw 25 kD), sodium alginate (Alg, Mw 12–80 kD) and poly(dially dimethyl ammonium chloride) (PDDA, Mw 100–200 kD) were purchased from Sigma-Aldrich (St. Louis, MO). NMR reagents were from Cambridge Isotope Laboratories, Inc. (Andover, MA). *S*-nitrosoglutathione (GSNO) and *S*-nitrosocysteine (CysNO) were freshly prepared as previously reported [12]. Phosphate buffered saline (PBS), pH 7.4, containing 137 mM NaCl, 2.7 mM KCl, 10 mM sodium phosphate, was used in all experiments. All solutions were prepared with deionized water from a Milli-Q system (18 MΩ cm^{-1}; Millipore Corp., Billerica, MA). *Pseudomonas aeruginosa* (*P. aeruginosa*) PAO300, a *mucA22* derivative of PAO1 that constitutively overproduce alginate [21] was obtained from the University of Copenhagen, Denmark. *Escherichia coli* (*E. coli*) K-12 MG16653 and *Staphylococcus aureus (S. aureus)* ATCC 45330 were purchased from American Type Culture Collection. Luria Bertani (LB) agar and broth were purchased from Fisher Scientific Inc. (Pittsburgh, PA).

2.2 Synthesis of C-ebselen and immobilization of C-ebselen on PEI

C-ebselen was synthesized using a reported method [22] with a minor modification of using anhydrous acetonitrile [23] instead of ether as the solvent in the third step. ^{1}H NMR, ^{13}C NMR spectra and mass spectra of C-ebselen were recorded using a Varian MR400 MHz, Varian VNMRS 700 MHz spectrometer and a VG (Micromass) 70–250-S Magnetic sector mass spectrometer (EI, 70eV), respectively.

^{1}H NMR (400 MHz, DMSO-d_6): δ 12.92 (s, 1H, -COOH), 8.11-8.09 (d, J=8.0 Hz, 1H, ArH), 8.02-7.99 (d, J=8.8 Hz, 2H, ArH), 7.93-7.91 (d, J=7.6 Hz, 1H, ArH), 7.86-7.84 (d, J=8.4 Hz, 2H, ArH), 7.72-7.69 (t, J=7.6, 1H, ArH), 7.51-7.48 (t, J=7.4 Hz, 1H, ArH). ^{13}C NMR (176 MHz, DMSO-d_6): δ 166.72, 165.33, 144.07, 138.65, 132.65, 130.48, 128.59,

128.10, 127.17, 126.41, 125.87, 123.39. EI-MS *m/z* $[M]^+$ calculated for $C_{14}H_9NO_3{}^{80}Se$, 319.0 (nominal mass), measured 319.1, measured isotope pattern matches predicted pattern for $C_{14}H_9NO_3Se$.

C-ebselen immobilized PEIs (e-PEI) with different Se contents were synthesized by EDC/NHS coupling of C-ebselen with PEI in pH 6.0 MES buffer. Carboxyl:-NH_2 molar ratios of 1:10 and 1:3 were selected for comparison studies. C-ebselen was first dissolved in MES buffer containing NaOH to form a clear yellow solution. EDC and NHS were then added to the solution (molar ratio -COOH: EDC: NHS=1:6:4) and the clear solution became turbid after 5 min. A PEI solution in MES was further added and the final pH was adjusted to 6.0. The reaction was kept at room temperature for 12 h. The reaction mixture was then centrifuged and the polymers in the supernatant were further dialyzed (MWCO, 2 kD) against 0.05 M NaCl for 2 d and then Milli-Q water for 1 d. The e-PEI obtained was then lyophilized and the Se content was determined by inductively coupled plasma - optical emission spectroscopy (ICP-OES) on a Perkin-Elmer Optima 2000 DV (Perkin-Elmer, Wellesley, MA) to be 1.87 wt% and 4.14 wt%, respectively, for the two different e-PEI preparations.

2.3 Labeling e-PEI and Alg with fluorophores

The e-PEI was labeled with RB and Alg was labeled with FTSC by EDC/NHS reaction for 12 h in MES buffer, pH 6.0, using molar ratio EDC: fluorophore: NHS: -NH_2/–COOH = 1:1:1:20. The labeled polymer was then washed and dialyzed extensively in dark before use.

2.4 Layer-by-Layer assembly of e-PEI/Alg

Glass and quartz slides were cleaned with piranha solution (7:3 H_2SO_4/30% H_2O_2) at 80 °C before use (*Caution: the solution is extremely corrosive!*) and the LbL films were prepared by alternately dipping the substrates in 1 mg mL^{-1} e-PEI and Alg solutions in pH 7.4 PBS (10 min each) with three intermediate PBS washings (1 min each) using a homemade automated deposition system until desired number of bilayers were assembled onto the substrate. The as prepared LbL films were further placed in a salt annealing solution (PBS buffer containing 1.5 M NaCl) for 1 min and then cross-linked for 12 h in a cross-linking solution (PBS buffer containing 1.5 M NaCl and EDC/NHS 50 mM).

2.5 Characterization of LbL films

2.5.1 UV-Vis spectra—The UV-Vis spectra of LbL films on quartz slides were recorded on a UV-Vis spectrophotometer (Lambda 35, Perkin-Elmer, MA). The quartz slides were placed vertically into a quartz cuvette containing 3 mL buffer solution and the UV-Vis spectra were recorded with a data interval of 1 nm. To record the spectra of the film after salt annealing, the film was placed in the salt annealing solution for 1 min and then transferred to another cuvette containing the annealing solution for recording the spectra.

2.5. 2 NO generation detection—The catalytically generated NO from the LbL coatings was detected by purging N_2 into 2 mL pH 7.4 PBS solution in an NOA cell protected from light and monitored using a chemiluminescence NO analyzer (NOA) (Sievers 280, Boulder, CO). For the homogeneous experiments with different organoselenium species, the Se-based catalysts were dissolved in DMSO while reducing agent and RSNOs were freshly prepared in pH 7.4 PBS to form 5 mM solutions, respectively. Lyophilized e-PEI was dissolved as a 1 mg mL^{-1} solution in PBS. Glass slides with LbL coatings were soaked in PBS containing 100 μM EDTA, 100 μM GSH overnight before the NOA test. To monitor the superoxide scavenging effect, air instead of N_2 was used for the purging.

2.5.3 Scanning electron microscopy—Scanning electron microscopy (SEM) images were recorded on a Hitachi S-3200N scanning electron microscope (Hitachi High Technologies, Tokyo, Japan) at a working distance of 15 mm at 16 kV. Glass slides with the LbL coatings were dip-washed with Milli-Q water, dried in a desiccator overnight and then sputter-coated with gold for 30 s before imaging.

2.5.4 Optical microscopy and confocal laser scanning microscopy—Glass slides with LbL coatings were placed in CoverWell perfusion chambers (Sigma-Aldrich, St. Louis, MO) containing PBS buffer or the salt annealing solution for solution phase imaging. Optical microscopy images were recording on a Nikon Eclipse E600 POL optical microscope (Nikon Instruments, Inc., Melville, NY) using a 20× or a 40× objective lens. A Zeiss LSM 510-META confocal laser scanning microscope (Carl Zeiss Microimaging, Inc., Thoronwood, NY) was used for recording confocal images in PBS buffer or annealing solutions. The fluorophores were excited by an Argon laser at 488 nm and a HeNe laser at 543 nm and observed with a C-Apochromat 63× objective lens using two filters (505–550 nm, 560 nm). The images were scanned at a speed of 1.6 μs/pixel using a 12 bit plane mode. The image size was 1024×1024 pixel, which corresponds to an area of 143 μm ×143 μm.

2.5.5 Selenium content and Se leaching tests—The LbL films on glass slides were digested using fuming nitric acid and further diluted to a 10 mL final volume and the Se content of the films was determined with inductively coupled plasma - optical emission spectroscopy (ICP-OES) on a Perkin-Elmer Optima 2000 DV (Perkin-Elmer, Wellesley, MA). The Se leaching test was done by placing a $(\text{e-PEI/Alg})_{100}$ film in 9 mL of PBS buffer containing 100 μM EDTA, 50 μM GSH and 50 μM GSNO at 37.5 °C in the dark for 24 h. Each day, the soaking solution was collected, diluted to 10 mL and replaced. After one week, the Se contents in the daily soaking solutions were measured with inductively coupled plasma high-resolution mass spectrometry (ICP-HRMS), using a Thermo Finnigan Element (Thermo Electron Corp., Schaumberg, IL).

2.6 *In-vitro* blood test

Fresh heparinized (5 U mL^{-1}) sheep whole blood was obtained from Extracorporeal Membrane Oxygenation (ECMO) Laboratory in the Medical School at the University of Michigan. The blood was centrifuged at 1300 rpm for 15 min to obtain platelet-rich sheep plasma (PRP). LbL films were assembled onto Kendall monoject veterinary polyurethane (PU) I.V. catheters (Tyco Healthcare) or glass slides by the automatic LbL coating system and annealed using the method outlined above. Three catheters with annealed LbL coatings were then placed in PBS buffer, sheep plasma and sheep whole blood for 24 h at 4 °C, respectively. The catheters were dip washed by PBS before testing NO generation from RSNOs with NOA. The NO generation from a solution of pH 7.4 PBS containing 100 μM EDTA, 10 μM CysNO and 20 μM CySH at 37.5°C was monitored using the method described in 2.5.2. Six glass slides with the same LbL coatings were also used for the experiment (duplicate for each soaking experiment) and after the NOA test, the LbL film on glass slides was digested by fuming nitric acid and the Se content was determined by ICP-OES.

2.7 Detection of superoxide production from LbL films

Superoxide produced from the LbL films constructed with e-PEI was detected using a previously reported lucigenin-derived chemiluminescence assay via a Shimadzu RF-1501 spectrofluorophotometer (Shimadzu, Columbia, MD) [24]. Forty μL of 6.25 mM lucigenin (in DMSO) solution was mixed in 960 μL of glycine-NaOH buffer (0.05 M, pH=10) in semimicro disposable cuvettes. Annealed $(\text{e-PEI/Alg})_{50}$, annealed $(\text{PEI/Alg})_{50}$ and $(\text{PDDA/Alg})_{50}$ films on glass slides were presoaked in 100 μM EDTA and 100 μM GSH PBS buffer

overnight and then placed in the cuvettes to record the emission spectra. The chemiluminescence signal from 350–650 nm was integrated and the integrated intensity per unit area of the films was compared.

2.8 *In-vitro* antimicrobial tests

Glass slides coated with LbL films were presoaked in PBS buffer containing 100 μM EDTA and 100 μM GSH before the antimicrobial tests to remove the interference from trace metal ions and reduce the catalytic sites into the selenolate form. Overnight LB-broth grown bacterial culture was washed with PBS buffer three times, and resuspended in PBS buffer to make a final cell concentration at 10^5 or 10^8 CFU/mL, respectively. For solution phase antimicrobial tests, LbL films coated glass slides were placed into a Corning 15-mL tube with 2 mL of washed bacterial culture with or without addition of GSH solution. The tube was incubated at 37.5 °C for 2 h or 24 h with horizontally shaking at 150 rpm. After incubation, coated slide was removed and the bacterial culture was serially 10-fold diluted in PBS buffer and 50 μL of each dilution was plated onto LB (Luria Bertani) agar plate for viable bacterial counting. Annealed $(\text{e-PEI/Alg})_n$, annealed $(\text{PEI/Alg})_{50}$ and glass controls in bacterial solution containing 0 or 20 μM GSH were used to study the effect of bilayer numbers, while annealed $(\text{e-PEI/Alg})_{50}$, annealed $(\text{PEI/Alg})_{50}$ and glass controls in bacterial solution containing 0, 20 or 50 μM GSH were used to study the effect of different concentrations of reducing agent. Annealed $(\text{e-PEI/Alg})_{50}$ and glass controls were also used to study the influence of specific strains of different bacteria (including *E. coli*, *P. aeruginosa* and *S. aureus)* on the antimicrobial properties of the LbL films and the influence of RSNO addition. All the antimicrobial tests were done in duplicate.

For microscopic observation, glass slides with the annealed LbL films were placed in semimicro disposable cuvettes and 0.5 mL of washed bacterial culture was added to a final cell concentration of 10^5 CFU/mL. GSH was added to reach a final concentration of 50 μM. The solution was incubated at 37.5 °C for 2 h with horizontally shaking at 150 rpm. After incubation, LbL coated slides were removed and stained with fluorescent dyes (SYTO-9 and propidium iodide) for 20 min in dark according to the instruction of LIVE/DEAD® BacLight™ Bacterial Viability kit (L7012, Invitrogen, Carlsbad, CA). Stained slides were observed with a fluorescence microscope (Olympus 1×71, Center Valley, PA) equipped with Fluorescence Illumination System (X-Cite 120, EXFO) and appropriate filter sets. Images were obtained using an oil immersion 60 × objective lens. Untreated glass slides were used as controls. Three images were taken for the same film and used for quantitative analysis. The images were analyzed using COMSTAT software (version 1) [25] with the threshold setting as 25 and the surface bacterial coverage and deal cell percentage for glass slide, $(\text{PEI/Alg})_{50}$ and $(\text{e-PEI/Alg})_{50}$ were compared.

3. Results and Discussion

3. 1 Identifying the key intermediate for C-ebselen catalytic activity

Before working with LbL films, the homogeneous catalytic activity of C-ebselen for RSNO decomposition was studied using GSH as the reducing agent at pH 7.4 PBS. EDTA was added to eliminate the interference from free metal ion-induced RSNO decomposition. As shown in Fig. 2a–B and 2b-B, this compound is able to generate NO from both GSNO (a) and CysNO (b). It has been reported that selenol or selenolate is the key intermediate for the RSNO decomposition by organodiselenide species [12]. For ebselen, the reaction with equal molar of GSH will first produce a GSH-selenenyl sulfide product, which will be further reduced to ebselen selenol in the presence of excess GSH (see reactions in Supporting Information Fig. 1S-a). The presence of an ebselen selenol intermediate has been verified elsewhere [26]. The pKa is ca 5.5 for aliphatic selenols [12], and an arylselenol should have

an even lower pKa due to reduced electron density on selenium atom. Therefore, at pH 7.4, in the presence of excess GSH, C-ebselen is in its selenolate form. In a homogeneous experiment in which different amounts of free C-ebselen catalyst were added into a solution containing 100 μM EDTA, 50 μM GSNO and 50 μM GSH, it was found that the NO generation was fastest when the molar ratio of GSH:C-ebselen = 2:1(Supporting Information Fig. 1S-b). When the molar ratio of GSH:C-ebselen was kept at 2:1, it was also found that the NO generation rate increased linearly with selenolate concentration (Supporting Information Fig. 1S-c). Therefore, C-ebselen selenolate is expected to be the key intermediate for the RSNO decomposition activity.

3. 2 Comparison of RSNO decomposition activity of SeDPA, C-ebselen and ebselen

The catalytic activity of SeDPA, C-ebselen and ebselen towards GSNO and CysNO decomposition was compared and shown in Fig. 2a and Fig. 2b. When the selenolate concentrations are kept the same for all three catalysts, SeDPA exhibits the best catalytic activity. This is because aliphatic selenolates are better nucleophiles compared to aromatic ones due to the higher electron density on the Se atom. The reduced steric hindrance owing to the smaller size of the SeDPA selenolate also contributes to the improved catalytic activity (see structures in Fig. 2c). C-ebselen, however, exhibits much better catalytic activity than ebselen. It is possible that this improvement arises from the better solubility of C-ebselen-selenolate in aqueous phase coming from the ionization of the carboxyl group at neutral pH. When CysNO, a smaller RSNO with less steric hindrance was used instead of GSNO, improved catalytic activity is observed for both C-ebselen and ebselen.

3. 3 Catalytic activity of e-PEI

Ebselen-PEIs with different C-ebselen to $-NH_2$ molar ratios were synthesized and the Se contents of the polymers were calculated from ICP-OES to be 1.87 wt% (e-PEI-2) and 4.14 wt% (e-PEI-4), respectively. Fig. 3a insert shows the UV-Vis spectra of PEI (A), e-PEI-2 (B) and e-PEI-4 (C) at the same concentration (67 μg mL^{-1}) in pH 7.4 PBS buffer. Due to the introduction of ebselen segments, the spectra of e-PEI solutions exhibit two bands. While the absorption at 280 nm is from the benzene ring, the absorption band at 350 nm is from the isoselenazol ring of the ebselen segments [27]. The ratio of C-ebselen moieties in the polymers calculated from the absorption differences at 280 nm was 2.2, which is consistent with the ICP results.

The catalytic activity of e-PEI-2, e-PEI-4 and free C-ebselen were compared in pH 7.4 PBS containing 100 μM EDTA and 50 μM GSNO. The selenolate concentration was kept at 50 μM for both polymers and C-ebselen. As shown in Fig. 3a, while e-PEI-2 shows catalytic activity equivalent to free C-ebselen, e-PEI-4 with a higher Se content, exhibits reduced catalytic activity. A proposed mechanism for the reduced catalytic activity is shown in Fig. 3b. It is possible that as the hydrophobic ebselen segments become denser (from higher C-ebselen loading on to polymer), the conformation of the amphiphilic e-PEI polymer will change in solution to form hydrophobic centers that prevent the access of GSH and GSNO to the catalytic sites. In this case, not all the catalytic sites in e-PEI-4 can be fully used for catalytic RSNO decomposition, which may contribute to the reduced catalytic activity observed for this species. Since e-PEI-2 has better catalytic activity, it was used to fabricate all the LbL films reported herein.

3. 4 Fabrication and annealing of LbL film

The initially prepared LbL films exhibit a cloudy appearance (Fig. 4, insert A) and are not stable. As shown in Fig. 5a-A, as soon as an unannealed $(e\text{-}PEI/Alg)_{50}$ is placed in PBS buffer containing 100 μM EDTA, 50 μM GSH and 50 μM GSNO, NO is generated due to the decomposition of RSNO by the catalytic sites in the LbL film. However, the NO

generation continues even after the film is removed, indicating significant leaching of catalytic sites from the film into the reaction reservoir. The leaching is attributed to the heterogeneous nature of the unannealed film. As shown in Fig. 4A, the UV-Vis spectrum of an unannealed $(e\text{-}PEI/Alg)_{50}$ exhibits large background signal from 400 nm to 700 nm, resulting from the light scattering of the heterogeneous film [28]. The heterogeneous nature of the unannealed film is further revealed by SEM images shown in Fig. 6A and 6B. The surface of the unannealed film is very rough, and it is composed of both vermiculate structures and particles. Based on this surface morphology, it is highly unlikely that the film is in a thermodynamically stable state. When this type of film is placed in solution for catalytic NO generation, chain rearrangements will take place to form a thermodynamically more stable structure, resulting in the leaching of the selenium species.

Layer-by-layer assembly, as indicated by Yang, et al., contains two steps: absorption and chain rearrangement [28]. While the former is a kinetically driven process that helps build the films, it also creates defects and results in thermodynamically unstable structures. Chain rearrangement, on the other hand, helps in healing the defects, but is a slow and inefficient process.

To obtain a more robust and stable LbL film, it is necessary to heal the defects and change the heterogeneous nature of the initial film. Therefore, the mobility of the polymer chains within the LbL film must be enhanced, and chain rearrangements have to take place to form a more homogeneous structure, which needs to be further stabilized. Based on this, a two-step annealing method was used to improve the stability of the LbL film and thereby to minimize the leaching of catalytic sites. As shown in Fig. 7, in the first step of annealing, salt is used to partly break the ionic bonds, enhance the chain mobility of the polyelectrolytes and turn a heterogeneous film into a homogeneous one. In the second step, EDC/NHS is added to the annealing solution, so that the ionic bonds within the homogeneous film are turned into covalent linkages and the film is “locked” in its homogeneous state.

Salt-induced annealing is a convenient, universal and effective method to improve the homogeneity of LbL films. When placed in the annealing solution, the unannealed $(e\text{-}PEI/Alg)_{50}$ turned from cloudy to clear within 1 min (Fig. 4, insert B). In addition, the background absorption in the UV spectra went back to zero (Fig. 4B) after the salt annealing, indicating the formation of a homogeneous film. However, if the salt concentration is less than 1.5 M, the film remains cloudy. Since salt anneals the surface by temporarily breaking the electrostatic contacts and smoothing the surface, the change will not happen immediately unless the salt concentration reaches certain level to break enough contacts [29]. To monitor the surface morphology change in solution during the annealing process, e-PEI and Alg were labeled with fluorophores and the surface morphology of the LbL films under different treatments were monitored using a confocal laser scanning microscope. As shown via the confocal images in Fig. 8A, in PBS buffer, an unannealed $(e\text{-}PEI/Alg)_{50}$ shows a rough surface containing significant aggregates of micro-particle-domains. The morphology of e-PEI (red) and Alg (green) are the similar to each other, indicating the formation of polyion pairs throughout the film. The surface morphology of the film in PBS buffer is different from the dry state SEM images shown in Fig. 6A-B, and this can be attributed to the polyelectrolyte conformation change from a stretched to a coiled conformation due to the reduced repulsion from the screening effect of salt [30]. When the same film is placed in the salt annealing solution, the surface becomes smooth immediately as shown in Fig. 8B. With the breakage of the ionic bonds, the microparticle domains are dissociated, allowing new and lower energy configurations to form. The salt annealing effect at solution phase is also observed by an optical microscope (shown in Supporting

Information Fig 2S. A–B), and this is similar to a previously reported smoothing effect from salt annealing [29].

Although salt-annealing produced more homogeneous LbL films, the films were fragile and swelled considerably after extended exposure to the annealing solution. Therefore, it is necessary to cross-link the film immediately after brief exposure. The cross-linking process is to "lock" the film in its homogeneous state by turning the ionic bonds into covalent linkages. However, cross-linking alone does not produce a stable film. As shown in Fig. 5a–B, an $(e\text{-PEI/Alg})_{50}$ film treated only by cross-linking shows similar NO generation pattern to an unannealed film, indicating that cross-linking alone does not solve the leaching problem. However, for a film treated with the two-step annealing process (Fig. 5a-C), the NO detection signal goes back to nearly baseline once the film is removed from the reaction reservoir, indicating minimal leaching of Se species. The NO flux of the annealed film, however, is lower than the unannealed one. This is consistent with a decrease in the Se contents for the LbL films after the annealing treatment (Supporting Information Fig. 3S-a). Therefore, the reduced NO flux is attributed to reduction in the total amount of e-PEI absorption resulting from the increased screening of surface charges in a highly concentrated salt solution [31]. The surface morphology of the film with cross-linking only and the annealed films are compared in SEM images in Fig. 6. As shown in Fig. 6C, similar to the surface morphology of unannealed $(e\text{-PEI/Alg})_{50}$ in PBS buffer shown in Fig. 8A, the surface of $(e\text{-PEI/Alg})_{50}$ treated by cross-linking only possesses significant micro-particle aggregations. This is further proof that cross-linking alone can "lock" the film morphology in solution phase by turning ionic bonds into covalent linkages. Although the cross-linking restricts the chain mobility of LbL films, due to the rough surface and structural instability, the cross-linked film still suffers from significant leaching problem. The annealed film, on the other hand, shows a flat and smooth surface as shown in Fig. 6D. At higher magnification (Fig. 6E), the entire film reveals a porous 3D structure, which is a thermodynamically stable network with minimal leaching. The film thickness for $(e\text{-PEI/Alg})_{50}$ is 3.5 μm (see Fig. 6F). The porous structure of the annealed film in PBS buffer is also observed by confocal microscope images shown in Fig. 8C, indicating the consistency of the surface morphology of the film in a dry state and in contact with a solution phase. The shift from a rough surface in PBS buffer to a smooth surface after the two-step annealing is also confirmed by optical microscope images shown in Supporting Information Fig. 2S-C. Compared to conventional LbL films, which are sensitive to environmental changes like pH and ionic strength, this type of film is a more stable and robust alternative.

3. 5 NO generation and Se leaching from annealed LbL films

The NO flux of the LbL films can be controlled by the number of bilayers that are incorporated into the films. As shown in Fig. 5b insert, the Se content of the LbL film grows exponentially with the number of bilayers within the films, which is consistent with a previously reported growth for a PEI/Alg LbL film [32]. In a PBS buffer containing 100 μM EDTA, 50 μM GSH, 50 μM GSNO, the NO flux of the LbL film increases with increased number of bilayers, as shown in Fig. 5b for $(e\text{-PEI/Alg})_{10}$, $(e\text{-PEI/Alg})_{30}$ and $(e\text{-PEI/Alg})_{50}$. However, when the catalyst content exceeds substrate amount, the increase in the NO flux is less obvious as shown for $(e\text{-PEI/Alg})_{50}$ and $(e\text{-PEI/Alg})_{100}$. In these cases, it is likely that most of the substrate is consumed by the outer layers before it reaches the inner layers and reacts with the inner catalytic sites. To investigate the stability of the LbL films, $(e\text{-PEI/Alg})_{100}$ with the highest Se content was repeatedly inserted and taken out of the reaction reservoir. As shown in Fig. 5c, no significant baseline signal increase is observed when the film is repeatedly taken out of the solution, indicating minimized leaching of Se species from the film.

The leaching of Se species from a $(e\text{-}PEI/Alg)_{100}$ film was monitored every day for a week using ICP-MS and the Se daily leaching was found to be 0.15~0.4 μg cm^{-1} (Supporting Information, Fig. 3S-b). Considering the small area of most medical devices, this value is far below the daily recommended intake of Se of 40 μg d^{-1} [13].

3. 6. *In-vitro* blood soaking experiment for annealed LbL films

One of the advantages of LbL coatings lies in that they are applicable to a variety of substrates. To determine whether the C-ebselen-based LbL films are potentially useful as coatings for blood contacting medical devices, the LbL films were assembled onto polyurethane (PU) catheters (shown in Fig. 5d, insert) and the NO fluxes of the catheters after 24 h soaking in PBS buffer, sheep plasma and whole sheep blood were compared. As shown in Fig. 5d-A, in the presence of 20 μM CySH and 10 μM CysNO at 37.5 °C, an $(e\text{-}PEI/Alg)_{50}$ coating on a polyurethane catheter with PBS soaking exhibits an NO flux of 5.5×10^{-10} mol cm^{-2} min^{-1} and the NO flux is 3×10^{-10} mol cm^{-2} min^{-1} for the film soaked in sheep plasma (Fig. 5d-B) or whole blood (Fig. 5d-C). To identify the reasons that contribute to the NO flux drop after blood or plasma soaking, the same experiments were conducted with $(e\text{-}PEI/Alg)_{50}$ on glass slides and NO fluxes and the Se contents of films after different treatments were compared (Supporting Information Fig. 4S). Although the films retain more than 80% of the total catalytic sites after plasma or blood soaking, the NO flux is only 55~ 60% of films that are only soaked in PBS buffer. Therefore, the reduced NO flux is likely due to the combination of a loss of catalytic sites and protein absorption on the LbL surfaces after plasma or blood soaking. In particular, protein absorption might block the catalytic sites from interacting with thiols and RSNOs, and it might also scavenge NO generated from the films through nitrosation of the thiol groups. However, considering healthy endothelial cells with the most antithrombotic surfaces produce NO fluxes of $0.5\sim4\times10^{-10}$ mol cm^{-2} min^{-1} [8], the LbL-film-based catheters are still able to generate physiological level of NO even after blood soaking for 24 h, indicating their potential antithrombotic properties.

3. 7 Antimicrobial properties of annealed LbL films

The antimicrobial effect of aliphatic selenium species-based films have been reported and it is believed that superoxide ($O_2^{\bullet-}$) produced from the reaction of aliphatic selenolate with oxygen is responsible for the observed antimicrobial activity [13]. Due to reduced electron density on selenium atom, ebselen and its derivatives are reported to produce less superoxide, which also contributes to their reduced *in-vivo* toxicity [15]. Since superoxide is a potent antimicrobial agent which causes oxidation stress and DNA damage to bacterial cells, even a small amount of superoxide production could lead to observable antimicrobial effects. Therefore, the superoxide production from $(e\text{-}PEI/Alg)_{50}$ and $(PEI/Alg)_{50}$ was assessed by a previously reported lucigenin-derived chemiluminescence assay [24]. A $(PEI/Alg)_{50}$ control produces 37% of the superoxide that is produced by $(e\text{-}PEI/Alg)_{50}$ (Supporting Information, Fig. 5S), indicating the introduction of only a small percentage (1.87 wt% Se) of C-ebselen segments greatly increased the superoxide production of the polymer matrix. The reason for the superoxide production from the $(PEI/Alg)_{50}$ matrix without immobilized organoselenium sites is unknown. However, decreased superoxide production from the LbL film was observed by the EDTA pre-soaking procedure or replacing PEI with PDDA (Supporting Information, Fig. 5S), suggesting that trace metal ions that are strongly bound to PEI are responsible for the observed production of superoxide by the background LbL matrix components.

The antimicrobial effects of ebselen and its derivatives have been reported [16], and the effect is suggested to be related to the S-N bond within this species. Since ebselen tends to inhibit enzymes by interacting with their L-cysteine residues, the inhibition of enzymes such

as H^+-ATPase [18] are reported to be one possible mechanism for the antimicrobial activity of ebselen and its derivatives.

For LbL films with covalently attached ebselen segments, the antimicrobial effects are expected to be related to both superoxide production and the surface interactions of immobilized ebselen sites with bacterial cells. In addition, since polyelectrolytes films have been reported to have antimicrobial functions by interacting with cell membranes [33], the PEI/Alg backbone may also contributes to the antimicrobial effects observed with the LbL films. Among all the possible factors, only superoxide is likely to diffuse out of the LbL layer and kill the bacteria surrounding the LbL films in the bulk solution. Considering the small thicknesses of the LbL films (e.g., 3.5 μm for $(\text{e-PEI/Alg})_{50}$ as indicated by SEM image Fig. 6F) and the short lifetime of superoxide, the killing effects are expected to take place in the vicinity of the film or in a contact-killing mode. Therefore, both the antimicrobial properties of the LbL films in solution and the surface bacterial attachment were evaluated.

Solution-based antimicrobial tests were used to investigate the factors related to the antimicrobial effects of the annealed LbL films. $(\text{e-PEI/Alg})_n$, $(\text{PEI/Alg})_{50}$ and glass controls were placed in PBS buffer containing 10^5 CFU/mL *E. coli* for 2 h at 37.5 °C and aliquots of the solution were taken out to determine the viable bacterial counts in the solutions. Given that the presence of a reducing agent is important for the production of the selenolate form of ebselen, which is required for generation of superoxide, the influence of reducing agent concentration was also studied. As shown in Fig. 9, compared with the control glass slides, e-PEI/Alg films and $(\text{PEI/Alg})_{50}$ exhibit different levels of antimicrobial effects. Without the presence of a reducing agent, $(\text{e-PEI/Alg})_{10}$, $(\text{e-PEI/Alg})_{30}$ and $(\text{e-PEI/Alg})_{50}$ are able to kill 66.1%, 95.6% and 98.2% of living *E-coli* cells in solution compared to a glass control that exhibits no killing effect. The killing efficacy increases with the number of bilayers that are incorporated into the e-PEI/Alg films, indicating a dose-dependent antimicrobial effect. An increase in the bilayer number leads to more catalytic sites to produce superoxide, resulting in more bacteria killed in solution phase. A $(\text{PEI/Alg})_{50}$ control film is able to kill 72.2% of bacterial cells under the same condition, indicating the contribution from the polyelectrolytes backbone to the antimicrobial properties of the e-PEI/Alg films. However, considering the viable bacterial counts after the treatment with $(\text{e-PEI/Alg})_{50}$ film is only 6% of that for the $(\text{PEI/Alg})_{50}$, the increased superoxide production greatly improves the killing efficacy of the ebselen-based LbL films. In the presence of 20 μM GSH as the reducing agent, all the LbL films except the glass slide control exhibit better killing efficacy when compared to the case with no reducing agent added. For $(\text{e-PEI/Alg})_{50}$ placed in bacteria solutions containing 0, 20 and 50 μM GSH, it is clear that the killing efficacy increases with the reducing agent concentration in the solution. While 2 logs of killing (i.e., the number of viable cells was reduced from ~1.8×10^5 to ~3×10^3 CFU/mL) is observed for $(\text{e-PEI/Alg})_{50}$ film without reducing agent added, the killing effect is improved to 3 logs (i.e., the number of viable cells was reduced from ~2.4×10^5 to ~8×10^2 CFU/mL) with the addition of 50 μM GSH. The reducing agent that facilitates selenolate formation will also facilitate superoxide production, thereby enhancing the antimicrobial properties of the coating.

Considering most of the antimicrobial effects of the films are taken place near the surface, the surface bacterial attachment on $(\text{e-PEI/Alg})_{50}$, $(\text{PEI/Alg})_{50}$ and a glass slide control were compared after soaking in 10^5 CFU/mL *E. coli* for 2 h at 37.5 °C in the presence of 50 μM GSH. As shown in Fig. 10, although viable attached bacterial cells (indicated by green dots) are obvious on the surface of a bare glass (A) and $(\text{PEI/Alg})_{50}$ (B), they are hardly observed on the $(\text{e-PEI/Alg})_{50}$ (C) surface. Quantitative analysis indicates that $(\text{e-PEI/Alg})_{50}$ and $(\text{PEI/Alg})_{50}$ are able to reduce 87% (~8 times reduction) and 56% (~2 times reduction) of

total bacterial surface coverage compared to a glass slide (n=3, $p<0.01$, see supporting information, Fig. 6S-a). For both $(e\text{-PEI/Alg})_{50}$ and $(PEI/Alg)_{50}$ surfaces, more than 92% (n=3, $p<0.01$, see supporting information Fig. 6S-b) of total bacteria attached are dead or membrane damaged (indicated by red dots in Fig. 10), demonstrating the killing effect at the surface. The difference between $(e\text{-PEI/Alg})_{50}$ and $(PEI/Alg)_{50}$ for total bacterial attachment especially living bacterial attachment clearly indicates that the ebselen segments and superoxide production play important roles in improving the antimicrobial properties of the LbL films. It is likely that superoxide present in the vicinity of the film kills the bacterial cells before they reach and attach onto the surface, thus help to repel living bacterial cells and reduce total bacterial surface coverage.

The antimicrobial effect of the LbL films was also found to be time and bacteria type dependent. When $(e\text{-PEI/Alg})_{50}$ was placed in 10^5 CFU/mL *E. coli* at 37. 5 °C, it was found that all the bacteria were killed after 24 h (data not shown), indicating longer time exposure to superoxide helps to kill more bacteria in solution. To determine whether the antimicrobial effect is universal, $(e\text{-PEI/Alg})_{50}$ was placed in 10^8 CFU/mL of *E. coli*, *P. aeruginosa* and *S. aureus* for 24 h at 37.5 °C. The LbL films are able to kill a broad spectrum of bacteria and better killing efficacy has been found for Gram positive *S. aureus* compared with Gram negative *E. coli* and *P. aeruginosa* (see Supporting Information, Fig. 7S), suggesting that the cell membrane structures of the given bacteria also influence the killing efficacy by the LbL films. Considering that *P. aeruginosa*, *S. aureus* and *E. coli* are highly related to wound, catheter or urinary tract infections [1, 34], the C-ebselen based LbL films have promising prospects in biomedical applications where such infections occur.

3. 8 Scavenging effect of NO and superoxide ($O_2^{\bullet-}$)

Although the NO and superoxide ($O_2^{\bullet-}$) generation from the carboxyl-ebselen-based LbL film suggests that this type of film has potential application as both an anti-thrombus and antimicrobial coating, to use this type of film as a coating with dual functionality, it is necessary to consider the scavenging effect coming from the reaction of NO and superoxide ($O_2^{\bullet-}$). Recently, both modeling and experimental results suggest that the reaction between NO and superoxide ($O_2^{\bullet-}$), which is faster than the reaction between NO and oxygen, contributes to the reduced detection limit observed for a selenocystamine-based electrochemical RSNO sensor under ambient conditions compared to under nitrogen atmosphere [24]. To evaluate the "NO scavenging effect" from superoxide ($O_2^{\bullet-}$) production, the NO generation behaviors of the C-ebselen and $(e\text{-PEI/Alg})_{50}$ in pH 7.4 PBS containing 100 μM EDTA, 20 μM CySH and 10 μM CysNO at 37.5°C under N_2 atmosphere or air flow were compared and the results are shown in the Supporting Information Fig. 8S-a. While in the presence of air, the superoxide ($O_2^{\bullet-}$) production scavenges ~30% of the total NO produced by the free C-ebselen, it also reduced the NO flux of $(e\text{-PEI/Alg})_{50}$ to ~74% of the flux under the N_2 atmosphere. However, the microbial killing effects are similar when $(e\text{-PEI/Alg})_{50}$ films are placed in *E. coli* solution containing 100 μM EDTA, 20 μM CySH with or without 10 μM CysNO for 1 h (see Supporting Information, Fig. 8S-b) and this is attributed to the antimicrobial effect of both NO and peroxynitrite ($ONOO^-$), the product of NO and superoxide ($O_2^{\bullet-}$) reaction. Considering that significant levels of NO are still produced in the presence of ambient oxygen, it is likely that most of the anti-thrombotic and anti-microbial properties of the LbL films will be retained even in the presence of this reaction. Hence, the C-ebselen-based LbL films have potential to be used as dual functional coatings to prevent both thrombus formation and bacterial infection.

Conclusions

In this work, carboxyl-ebselen was used to generate NO from endogeneous RSNOs via a catalytic process. Further, a carboxyl-ebselen-based LbL film, exhibiting minimal selenium

leaching, was able to produce physiological levels of NO from RSNOs after soaking in blood for 24 h. The LbL film was also able to prevent living bacterial surface attachment and showed promising antimicrobial effects for a broad spectrum of bacteria. This type of film, exhibiting the potential for both antithrombotic and antimicrobial properties, may be useful to help resolve complications due to thrombus formation and bacterial infection associated with a wide range of biomedical devices.

Supplementary Material

Refer to Web version on PubMed Central for supplementary material.

Acknowledgments

This work was supported by the National Institutes of Health (EB-004527). The authors thank Kelly Koch from the Extracorporeal Membrane Oxygenation Laboratory at the University of Michigan Medical School for providing sheep blood used in this work, Bruce Donohoe from Microscopy&Image Analysis Laboratory at the University of Michigan for his assistance for the confocal microscope images, Paul Lennon in the Department of Chemistry in University of Michigan of providing the EI-MS spectra analysis for carboxyl-ebselen and Dr. Ted Hunston in the Department of Geology at the University of Michigan for providing the Se leaching analysis using ICP-HRMS.

References

1. Dwyer A. Surface-treated catheters-a review. Semin Dial. 2008; 21:542–6. [PubMed: 19000120]
2. Frost MC, Reynolds MM, Meyerhoff ME. Polymers incorporating nitric oxide releasing/generating substances for improved biocompatibility of blood-contactincy medical devices. Biomaterials. 2005; 26:1685–93. [PubMed: 15576142]
3. Knetsch MLW, Koole LH. New strategies in the development of antimicrobial coatings: the example of increasing usage of silver and silver nanoparticles. Polymers. 2011; 3:340–66.
4. Stevens KNJ, Croes S, Boersma RS, Stobberingh EE, van der Marel C, van der Veen FH, et al. Hydrophilic surface coatings with embedded biocidal silver nanoparticles and sodium heparin for central venous catheters. Biomaterials. 2011; 32:1264–9. [PubMed: 21093906]
5. Major TC, Brant DO, Reynolds MM, Bartlett RH, Meyerhoff ME, Handa H, et al. The attenuation of platelet and monocyte activation in a rabbit model of extracorporeal circulation by a nitric oxide releasing polymer. Biomaterials. 2010; 31:2736–45. [PubMed: 20042236]
6. Riccio DA, Dobmeier KP, Hetrick EM, Privett BJ, Paul HS, Schoenfisch MH. Nitric oxide-releasing S-nitrosothiol-modified xerogels. Biomaterials. 2009; 30:4494–502. [PubMed: 19501904]
7. Hetrick EM, Schoenfisch MH. Antibacterial nitric oxide-releasing xerogels: Cell viability and parallel plate flow cell adhesion studies. Biomaterials. 2007; 28:1948–56. [PubMed: 17240444]
8. Vaughn MW, Kuo L, Liao JC. Estimation of nitric oxide production and reaction rates in tissue by use of a mathematical model. Am J Physiol-Heart Circul Physiol. 1998; 274:H2163–H76.
9. Hetrick EM, Shin JH, Stasko NA, Johnson CB, Wespe DA, Holmuhamedov E, et al. Bactericidal efficacy of nitric oxide-releasing silica nanoparticles. ACS Nano. 2008; 2:235–46. [PubMed: 19206623]
10. Kroncke KD, Suschek CV. Adulterated effects of nitric oxide - Generating donors. J Invest Dermatol. 2008; 128:258–60. [PubMed: 18195740]
11. Williams DLH. The chemistry of S-nitrosothiols. Acc Chem Res. 1999; 32:869–76.
12. Cha W, Meyerhoff ME. Catalytic generation of nitric oxide from S-nitrosothiols using immobilized organoselenium species. Biomaterials. 2007; 28:19–27. [PubMed: 16959311]
13. Tran PL, Hammond Aa, Mosley T, Cortez J, Gray T, Colmer-Hamood Ja, et al. Organoselenium coating on cellulose inhibits the formation of biofilms by Pseudomonas aeruginosa and Staphylococcus aureus. Appl Environ Microbiol. 2009; 75:3586–92. [PubMed: 19346348]
14. Mugesh G, du Mont WW, Sies H. Chemistry of biologically important synthetic organoselenium compounds. Chem Rev. 2001; 101:2125–79. [PubMed: 11710243]
15. Mugesh G, Singh HB. Synthetic organoselenium compounds as antioxidants: glutathione peroxidase activity. Chem Soc Rev. 2000; 29:347–57.

16. Pietka-Ottlik M, Wojtowicz-Mlociiowska H, Kolodziejczyk K, Piasecki E, Mlochowski J. New organoselenium compounds active against pathogenic bacteria, fungi and viruses. Chem Pharm Bull (Tokyo). 2008; 56:1423–7. [PubMed: 18827382]

17. Chan G, Hardej D, Santoro M, Lau-Cam C, Billack B. Evaluation of the antimicrobial activity of ebselen: Role of the yeast plasma membrane H^+-ATPase. J Biochem Mol Toxicol. 2007; 21:252–64. [PubMed: 17912695]

18. Billack B, Santoro M, Lau-Cam C. Growth inhibitory action of ebselen on fluconazole-resistant candida albicans: role of the plasma membrane H^+-ATPase. Microb Drug Resist. 2009; 15:77–83. [PubMed: 19432523]

19. Boudou T, Crouzier T, Ren K, Blin G, Picart C. Multiple functionalities of polyelectrolyte multilayer films: new biomedical applications. Adv Mater. 2010; 22:441–67. [PubMed: 20217734]

20. Yang J, Welby JL, Meyerhoff ME. Generic nitric oxide (NO) generating surface by immobilizing organoselenium species via Layer-by-Layer assembly. Langmuir. 2008; 24:10265–72. [PubMed: 18710268]

21. Mathee K, Ciofu O, Sternberg C, Lindum PW, Campbell JI, Jensen P, et al. Mucoid conversion of Pseudomonas aeruginosa by hydrogen peroxide: a mechanism for virulence activation in the cystic fibrosis lung. Microbiology. 1999; 145 (Pt 6):1349–57. [PubMed: 10411261]

22. Liu Y, Li B, Li L, Zhang HY. Synthesis of organoselenium-modified beta-cyclodextrins possessing a 1,2-benzisoselenazol-3(2H)-one moiety and their enzyme-mimic study. Helv Chim Acta. 2002; 85:9–18.

23. Młochowski J, Kloc K, Syper L, Inglot AD, Piasecki E. Aromatic and azaaromatic diselenides, benzisoselenazolones and related compounds as immunomodulators active in humans: synthesis and properties. Liebigs Ann Chem. 1993; 1993:1239–44.

24. Hofler L, Meyerhoff ME. Modeling the effect of oxygen on the amperometric response of immobilized organoselenium-based S-Nitrosothiol sensors. Anal Chem. 2011; 83:619–24. [PubMed: 21230000]

25. Heydorn A, Nielsen AT, Hentzer M, Sternberg C, Givskov M, Ersboll BK, et al. Quantification of biofilm structures by the novel computer program COMSTAT. Microbiology. 2000; 146:2395–407. [PubMed: 11021916]

26. Cotgreave, Ia; Morgenstern, R.; Engman, L.; Ahokas, J. Characterisation and quantitation of a selenol intermediate in the reaction of ebselen with thiols. Chem Biol Interact. 1992; 84:69–76. [PubMed: 1394616]

27. Haenen G, Derooij BM, Vermeulen NPE, Bast A. Mechanism of the reaction of ebselen with endogenous thiols: dihydrolipoate is a better cofactor than glutathione in the peroxidase activity of ebselen. Mol Pharmacol. 1990; 37:412–22. [PubMed: 2107391]

28. Yang S, Zhang Y, Zhang X, Guan Y, Xu J, Zhang X. From cloudy to transparent: chain rearrangement in hydrogen-bonded layer-by-layer assembled films. Chemphyschem. 2007; 8:418–24. [PubMed: 17183526]

29. McAloney, Ra; Dudnik, V.; Goh, MC. Kinetics of salt-induced annealing of a polyelectrolyte multilayer film morphology. Langmuir. 2003; 19:3947–52.

30. Fery A, Schöler B, Cassagneau T, Caruso F. Nanoporous thin films formed by salt-induced structural changes in multilayers of poly (acrylic acid) and poly (allylamine). Langmuir. 2001; 17:3779–83.

31. Ghannoum S, Xin Y, Jaber J, Halaoui LI. Self-assembly of polyacrylate-capped platinum nanoparticles on a polyelectrolyte surface: Kinetics of adsorption and effect of ionic strength and deposition protocol. Langmuir. 2003; 19:4804–11.

32. Ji J, Shen J. Electrostatic self-assemble and nanomedicine. Conf Proc IEEE Eng Med Biol Soc. 2005; 1:720–2. [PubMed: 17282284]

33. Lichter JA, Van Vliet KJ, Rubner MF. Design of antibacterial surfaces and interfaces: polyelectrolyte multilayers as a multifunctional platform. Macromolecules. 2009; 42:8573–86.

34. van der Starre WE, van Nieuwkoop C, Paltansing S, van't Wout JW, Groeneveld GH, Becker MJ, et al. Risk factors for fluoroquinolone-resistant Escherichia coli in adults with community-onset febrile urinary tract infection. J Antimicrob Chemother. 2011; 66:650–6. [PubMed: 21123286]

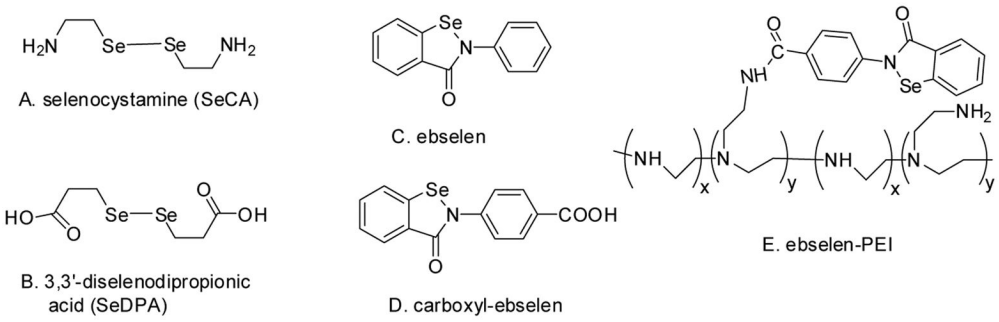

Fig. 1.
Structures of organoselenium species.

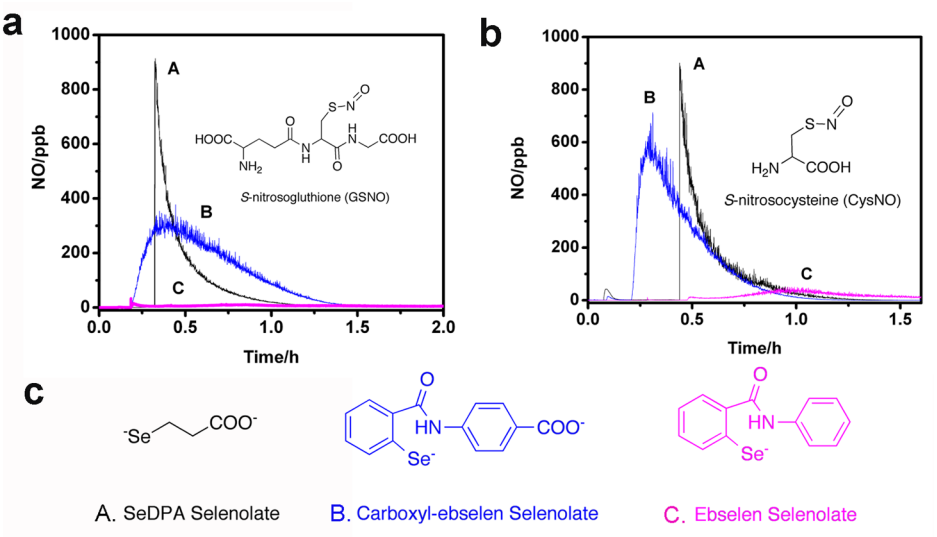

Fig. 2.

Catalytic NO generation profiles indicating comparison of the RSNO decomposition catalytic activity of C-ebselen, SeDPA and ebselen in homogeneous solution with 100 μM EDTA, 50 μM selenolate and 50 μM a) GSNO b) CysNO c) structures of selenolate of A) SeDPA B) C-ebselen C) ebselen.

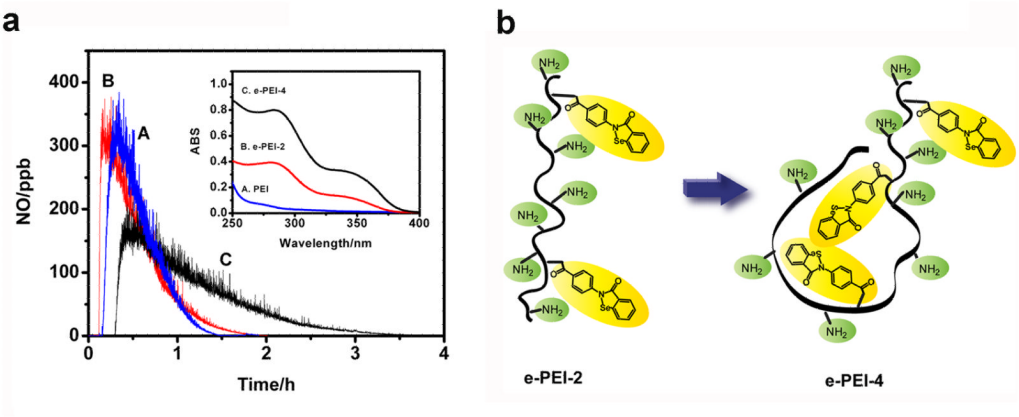

Fig. 3.

a) Catalytic NO generation profiles indicating comparison of RSNO decomposition catalytic activity of A) C-ebselen, B) e-PEI-2 C) e-PEI-4 in solution with 100 μM EDTA, 50 μM selenolate and 50 μM GSNO, insert shows the UV-Vis spectra of same concentration (67 μg/mL) of A) PEI, B) e-PEI-2, C) e-PEI-4 in PBS buffer b) schematic illustration of possibility of formation of hydrophobic centers in e-PEI-4 that prevent access of GSH and GSNO to the catalytic sites.

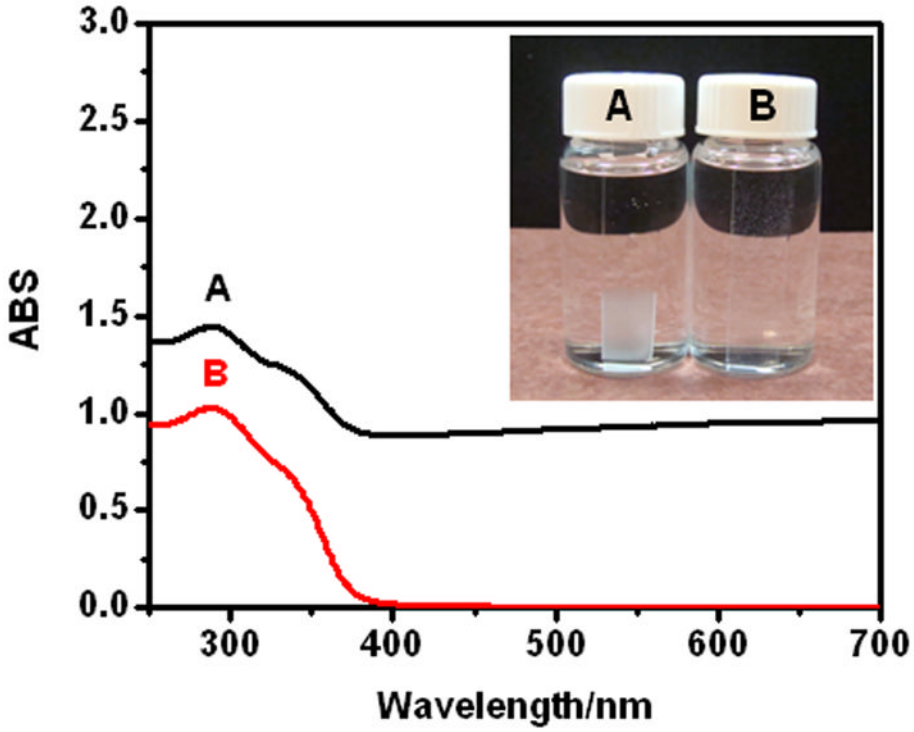

Fig. 4.

UV-Vis spectra of (e-PEI/Alg)$_{50}$ on quartz slides A) unannealed film in PBS and B) film after salt annealing in salt annealing solution. Insert shows the appearance of the films.

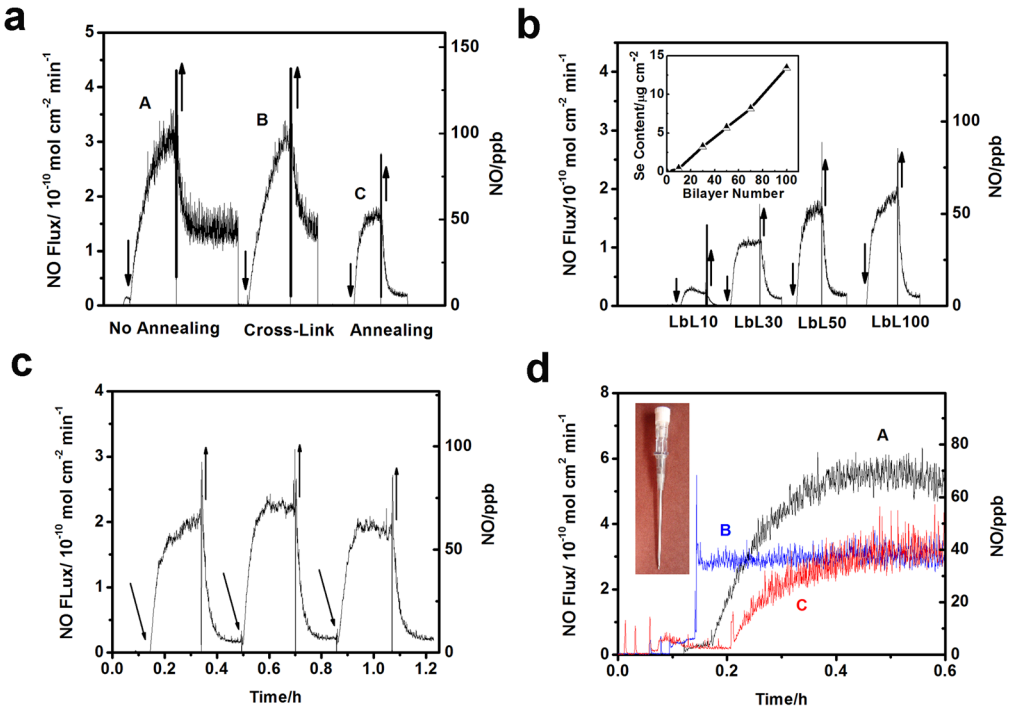

Fig. 5.

NO generation of a) $(e\text{-PEI/Alg})_{50}$ A) without annealing B) cross-link only C) after two-step annealing in 100 μM EDTA, 50 μM GSH, 50 μM GSNO at R.T., films are placed in and out of the NOA cell as indicated by ↓ and ↑ arrows. b) NO generation of LbL films with different bilayers on glass slides in 100 μM EDTA, 50 μM GSH, 50 μM GSNO at R.T. Insert: Se content of LbL films vs layer numbers. c) NO generation of $(e\text{-PEI/Alg})_{100}$ in 100 μM EDTA, 50 μM GSH, 50 μM GSNO at R.T. Film was repeatedly inserting and taken out of the solution as indicated by the ↑ and ↓arrows. d) NO generation from $(e\text{-PEI/Alg})_{50}$ on polyurethane catheters (insert) in 100 μM EDTA, 20 μM CySH, 10 μM CysNO at 37.5 °C after 24 h soaking in A) PBS B) sheep plasma C) sheep blood.

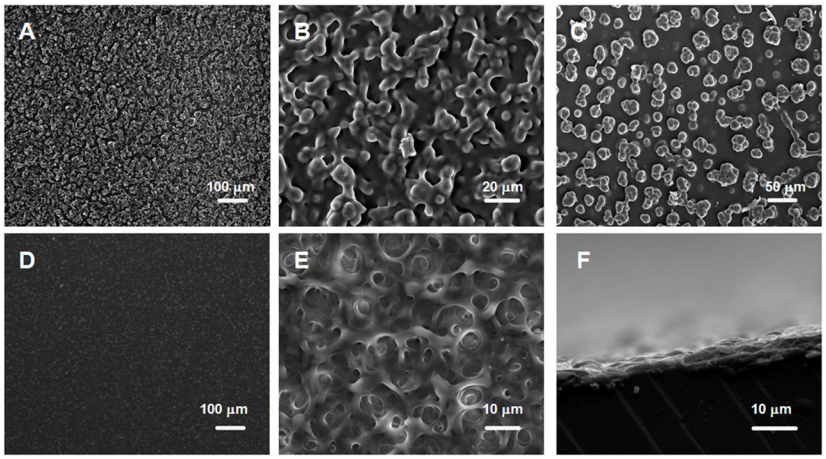

Fig. 6.

Scanning electron microscopy (SEM) images of (e-PEI/Alg)$_{50}$ A) B) without annealing C) cross-link only D) E) F) after two-step annealing.

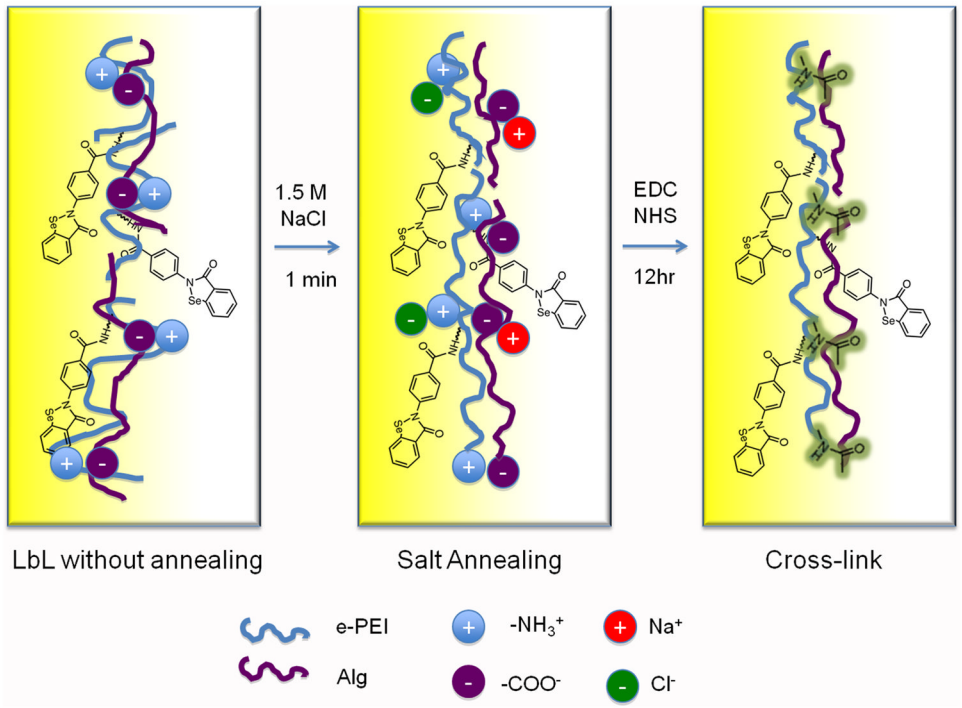

Fig. 7.
Schematic illustration of two step annealing of LbL films including salt annealing and cross-linking.

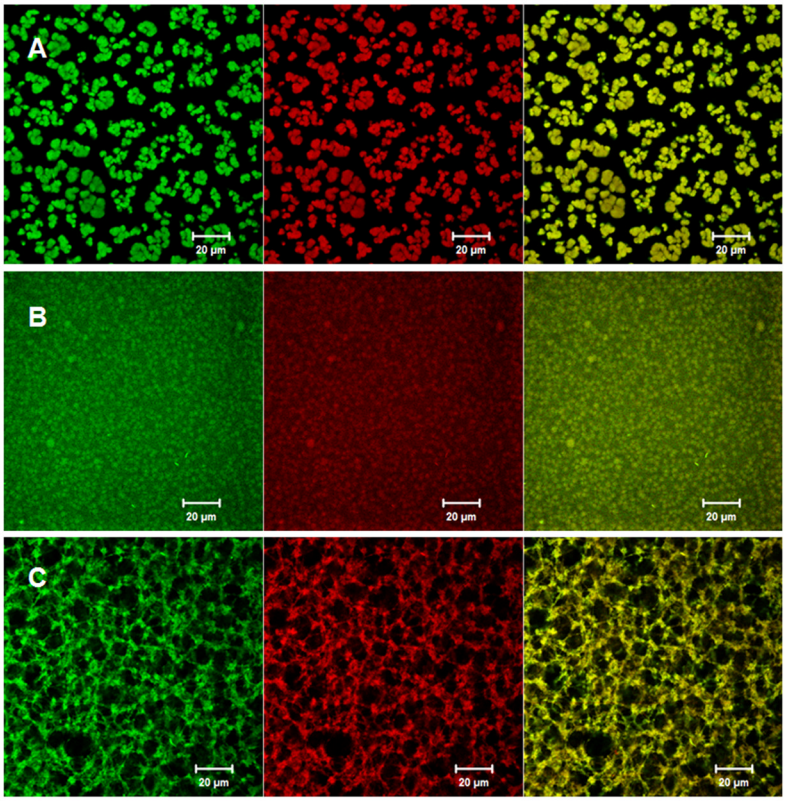

Fig. 8.

Confocal images of A) unannealed $(e\text{-PEI/Alg})_{50}$ in PBS B) $(e\text{-PEI/Alg})_{50}$ after salt annealing in PBS containing 1.5M NaCl C) $(e\text{-PEI/Alg})_{50}$ after two-step annealing in PBS, e-PEI (red), Alg (green).

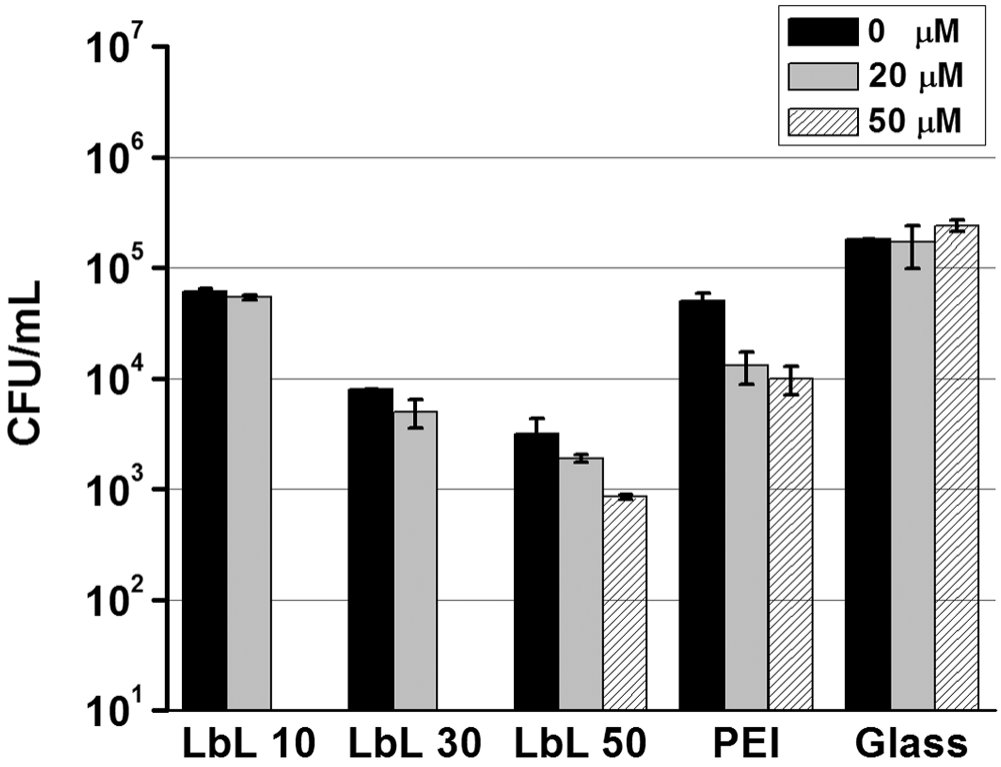

Fig. 9.

Effects of e-PEI/Alg film layer number and reducing agent concentration on the cell viability of *E coli*. $(\text{e-PEI/Alg})_{10}$, $(\text{e-PEI/Alg})_{30}$, $(\text{e-PEI/Alg})_{50}$, $(\text{PEI/Alg})_{50}$ and glass slides control were placed in 10^5 CFU/mL *E. coli* for 2 h at 37.5 °C with and without GSH as the reducing agent.

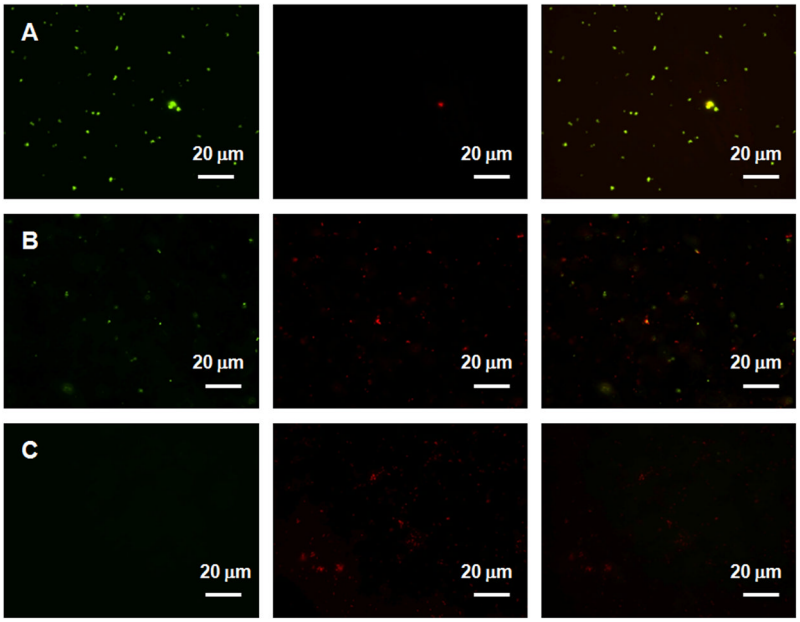

Fig. 10.

Representative fluorescent micrographs showing comparison of surfaces of A) bare glass B) $(e\text{-PEI/Alg})_{50}$ C) $(PEI/Alg)_{50}$ after soaking in 10^5 CFU/mL *E coli* containing 50 μM GSH for 2h at 37.5 °C. Bacterial cells were stained with Bacterial LIVE/DEAD staining dyes and viable cells shown green while dead or membrane damaged cells shown red fluorescence in the images.